Seasonal variations of the Na and Fe layers at the South Pole and their implications for the chemistry and general circulation of the polar mesosphere

Chester S. Gardner,[1] John M. C. Plane,[2] Weilin Pan,[1,3] Tomas Vondrak,[2] Benjamin J. Murray,[2,4] and Xinzhao Chu[1]

[1] Lidar observations, conducted at the South Pole by University of Illinois researchers, are used to characterize the seasonal variations of mesospheric Na and Fe above the site. The annual mean layer abundances are virtually identical to midlatitude values, and the mean centroid height is just 100 m higher for Na and 450 m higher for Fe compared with 40°N. The most striking feature of the metal profiles is the almost complete absence of Na and Fe below 90 km during midsummer. This leads to summertime layers with significantly higher peaks, narrower widths, and smaller abundances than are observed at lower latitudes. The measurements are compared with detailed chemical models of these species that were developed at the University of East Anglia. The models accurately reproduce most features of these observations and demonstrate the importance of rapid uptake of the metallic species on the surfaces of polar mesospheric clouds and meteoric smoke particles. The models show that vertical downwelling in winter, associated with the meridional circulation system, must be less than about 1 cm s^{-1} in the upper mesosphere in order to avoid displacing the minor constituents O, H, and the metal layers too far below 85 km. They also show that an additional source of gas-phase metallic species, that is comparable to the meteoric input, is required during winter to correctly model the Na and Fe abundances. This source appears to arise from the wintertime convergence of the meridional flow over the South Pole.

1. Introduction

[2] The presence of tenuous layers of neutral metal atoms in the upper atmosphere between about 75 and 110 km altitude has been known for more than 70 years. The Na, Fe, K, Ca, and Li layers result from meteoric ablation, and all have been studied during the past 3 decades using resonance fluorescence lidar techniques. Since *Bowman et al.* [1969] made the first Na lidar measurements in England during the late 1960s, mesospheric Na, owing to its large resonant backscatter cross section and high column abundance, has been widely used to study middle atmosphere dynamics and chemistry. During the past 25 years, extensive Na observations have been conducted at several mid- and low-latitude

sites [e.g., *Megie and Blamont*, 1977; *Simonich et al.*, 1979; *States and Gardner*, 1999]. These measurements have provided crucial data for validating models of the gas-phase chemical reactions associated with Na species under mid-latitude atmospheric conditions [*McNeil et al.*, 1995; *Plane et al.*, 1999a, 1999b]. The first lidar detection of the Fe layer was reported by *Granier et al.* [1989] at 40°N latitude. *Kane and Gardner* [1993] made extensive Fe and Na lidar measurements, also at 40°N, and reported that the annual mean Fe column abundance was approximately twice that of Na. More recently, *Raizada and Tepley* [2003] characterized the seasonal variations of the Fe layer at Arecibo (19°N). *Helmer et al.* [1998] developed a detailed model of Fe chemistry at mesopause heights and compared the model predictions with the observations of *Kane and Gardner* [1993].

[3] Until recently, only sporadic measurements of the mesospheric metal layers at high latitudes have been reported [*Nomura et al.*, 1987; *von Zahn et al.*, 1988; *Gardner et al.*, 1988; *Kurzawa and von Zahn*, 1990; *Alpers et al.*, 1990; *Collins et al.*, 1994; *Plane et al.*, 1998; *Gardner et al.*, 2001; *Kawahara et al.*, 2002; *Collins and Smith*, 2004]. The summer polar mesopause region is constantly illuminated by the Sun and is characterized by

---

[1]Department of Electrical and Computer Engineering, University of Illinois at Urbana-Champaign, Urbana, Illinois, USA.

[2]School of Environmental Sciences, University of East Anglia, Norwich, UK.

[3]Now at Center for Geospace Studies, SRI International, Menlo Park, California, USA.

[4]Now at Department of Chemistry, University of British Columbia, Vancouver, British Columbia, Canada.

extremely cold temperatures and the frequent occurrence of polar mesospheric clouds (PMCs). It has long been known that these cold temperatures are responsible for a significant reduction in mesospheric Na during the summer months in the Arctic [*von Zahn et al.*, 1988; *Gardner et al.*, 1988], in part because key chemical reaction rates depend strongly on temperature [e.g., *McNeil et al.*, 1995; *Plane et al.*, 1998]. In addition, *Plane et al.* [2004] have shown that the uptake of Fe on PMCs is rapid compared with the rate of meteoric ablation and vertical transport of Fe, so that the clouds effectively remove most of the Fe atoms in their vicinity. It has also been reported that K atoms are absent from the region occupied by PMCs [*Lübken and Höffner*, 2004], and the same behavior can be expected for Na atoms. Observations made during winter at the South Pole [*Pan et al.*, 2002; *Pan and Gardner*, 2003] and at Syowa (69°S) [*Kawahara et al.*, 2002, 2004] have revealed that the mesopause region is much colder and the vertical downwelling is much less than current model predictions. All of these conditions have an impact on the chemistry and structure of the metal layers.

[4] In this paper we use extensive Na and Fe lidar measurements, made by the University of Illinois during the past decade, to characterize for the first time, the seasonal variations of these mesospheric metal layers above the South Pole. The observations are compared with Na and Fe layer chemical models that were developed at the University of East Anglia. These models employ novel laboratory and numerical techniques to determine the key reaction rates [e.g., *Plane*, 2003; *Murray and Plane*, 2003]. The observations and models are used to gain new insights into the influence of temperature, vertical transport, meridional wind convergence, and gas-phase and heterogeneous chemistry on the seasonal structure of the Na and Fe layers at extremely high latitudes.

2. Observations

[5] In November 1994 the University of Illinois deployed a Na density lidar at the Amundsen-Scott South Pole Station. The system was designed to measure stratospheric aerosols and Na density profiles in the mesopause region. The lidar consisted of a 0.35-m-diameter telescope and a dye laser pumped by a frequency doubled Nd:YAG laser. Na layer observations began on 1 January 1995 and continued through 28 December 1997. Six-hundred-seventy-eight hours of Na measurements were obtained on 67 different days during the 3-year deployment. Summertime observations and detailed modeling studies of the temperature-dependent chemical reactions involving the Na species were reported by *Plane et al.* [1998]. In November 1999, the University of Illinois installed a Fe Boltzmann temperature lidar at the South Pole Station. This system was designed to measure stratospheric temperatures between 30 and about 70 km using the Rayleigh technique and Fe densities and temperatures between about 75 and 110 km using the Boltzmann technique [*Gelbwachs*, 1994; *Chu et al.*, 2002]. Starting on 2 December 1999 and continuing through 11 October 2001, more than 658 hours of Fe measurements were collected with this system on 92 different days throughout the year. *Pan and Gardner* [2003] characterized the seasonal variations of atmospheric tem-

peratures from the surface up to 110 km by combining the Fe/Rayleigh lidar measurements with high-altitude balloonsonde data. *Chu et al.* [2003] characterized the summertime PMC observations.

[6] During the austral summer season, PMCs are frequently observed in the high-latitude mesopause region. These thin layers of nanometer-size ice particles are formed through microphysical processes of nucleation-condensation-sedimentation under supersaturation conditions [e.g., *Avaste*, 1993; *Thomas*, 1991]. *Chu et al.* [2003] reported that the PMC occurrence frequency was 67.4% during summer at the South Pole. The mean PMC altitude was 85 km. In the presence of PMC, the lidar returns consist of resonance backscatter from Fe or Na atoms and Mie backscatter from cloud particles. The Fe Boltzmann lidar was designed to measure the atmospheric temperature by taking the ratio of the Fe fluorescence backscatter signal at two closely spaced resonance lines (372 and 374 nm) [*Gelbwachs*, 1994]. Because the PMC backscatter signals are nearly identical at these two wavelengths while the Fe signals are substantially different, the PMC signal can be eliminated from the 372-nm data by subtracting the 374-nm return signal and scaling the difference. The scaling factor depends on the known temperature-dependent relationship of the Fe backscatter signals at 372 and 374 nm. This approach permits the measurements of Fe densities even at the altitude of the PMCs [*Plane et al.*, 2004]. Because the Na lidar employs a single wavelength, it is not possible to compensate the Na profiles for contamination caused by PMC scattering. However, since the Na lidar employs a much longer wavelength (589 nm) and lower laser power, scattering from the nanometer-size PMC particles is much weaker (~factor 10–15) for the Na lidar compared to the Fe lidar. Even though PMCs are common at the South Pole during midsummer, the Na data employed in this study showed no evidence of PMC scattering below 90 km. Apparently the Na lidar was not sensitive enough to observe the PMCs.

[7] Plotted in Figure 1 are the weekly mean Na and Fe density profiles. The data were collected at a resolution of 48 m. The weekly mean density profiles were smoothed vertically with a 1-km FWHM (full-width-at-half-maximum) Hamming window to reveal the background structure of the Na and Fe layers and were then plotted at a vertical resolution of 500 m. There is a large gap in the Na data (~11 weeks) from late September to early December. The largest gap in the Fe data (~3 weeks) is from mid-October to early November. In the austral summer season when the mesopause region is extremely cold and PMCs are common between 80 and 90 km, both layers are narrow and their densities are low. There is little Na or Fe below 90 km in summer whereas in midwinter, both layers extend below 80 km. In late fall and early winter, the Na and Fe layers undergo tremendous growth and expansion. Sporadic layers of both metallic species were observed occasionally throughout the year.

[8] The column abundances, centroid heights, and RMS (root-mean-square) widths of Na and Fe layers are plotted versus month in Figures 2a–2f. The mean plus annual and semiannual harmonic fits to the data are also plotted as solid curves in Figure 2. Strong annual oscillations are observed in the layer abundances with minima in the summer months.
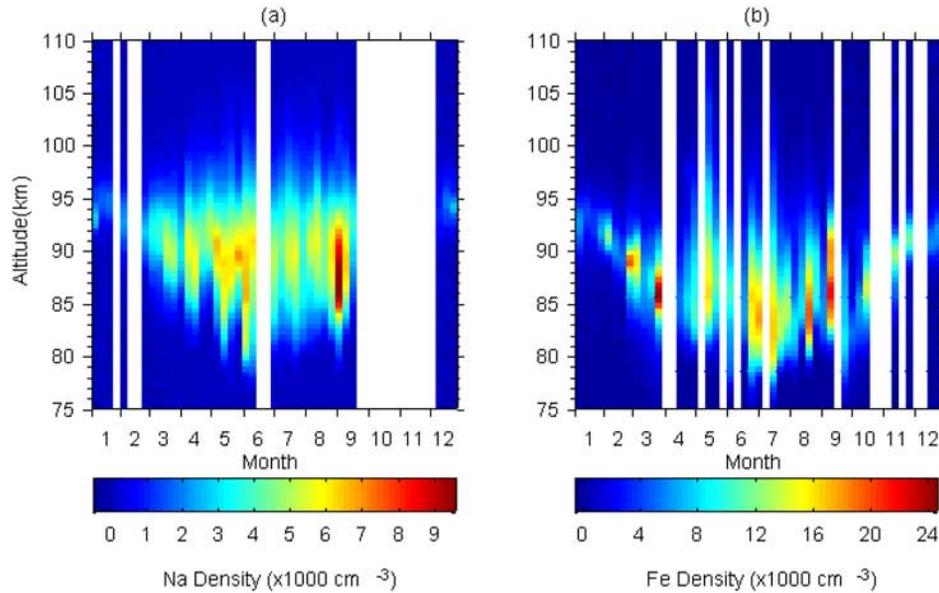
Figure 1. Weekly mean density profiles of the mesospheric (a) Na and (b) Fe layers observed at the South Pole. The vertical resolution is 500 m.

The Fe abundance is highly variable and ranges from 2.1×10^9 to 25.0×10^9 cm^{-2} with a mean of 9.7×10^9 cm^{-2}. The Na abundance varies from 0.3×10^9 to 11.0×10^9 cm^{-2} with a mean of 4.3×10^9 cm^{-2}. The Fe centroid height is between 84.0 and 94.6 km with a mean of 88.4 km, while the Na centroid ranges between 88.5 and 94.6 km with a mean of 91.5 km. The RMS width of the Fe layer ranges from 2.0 to 6.8 km with a mean of 4.2 km, and for the Na layer it ranges from 1.5 to 5.9 km with a mean of 3.7 km. The detailed characteristics of these layer parameters, including their means, 12-, and 6-month harmonics, are listed in Table 1. The abundances and widths of the Fe and Na layers exhibit similar seasonal variations. While these parameters are dominated by a 12-month oscillation, moderately strong 6-month oscillations are also present in the centroid height and RMS width variations of the Fe layer. In addition, both layers are highest and narrowest near summer solstice. This behavior is a consequence of the extremely low Fe and Na densities below 90 km in midsummer.
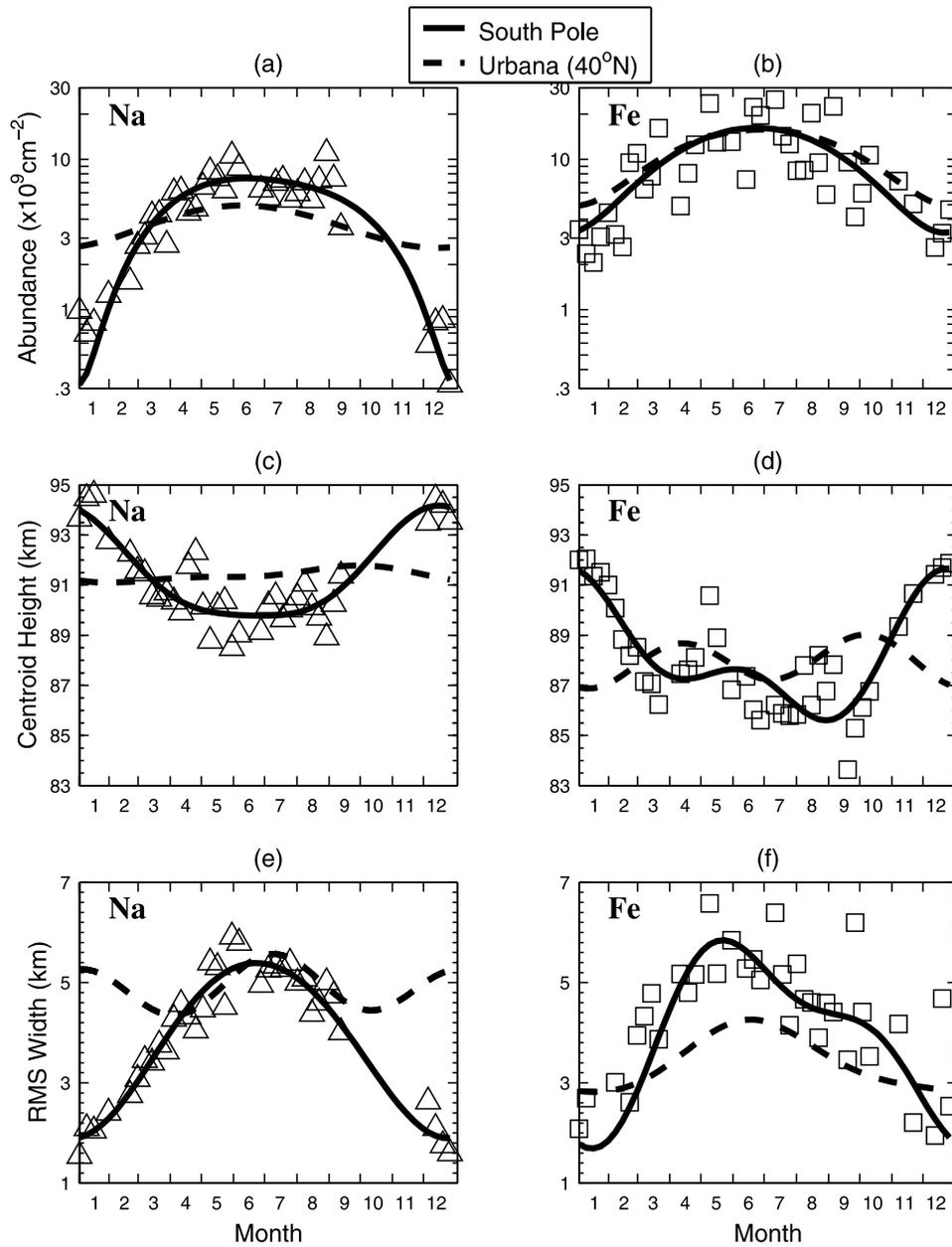
[9] For comparison, the seasonal harmonic fits for Fe and Na observations made at the Urbana Atmospheric Observatory (40°N) are also plotted as dashed curves in Figure 2 [*Kane and Gardner*, 1993; *States and Gardner*, 1999]. These fits have been shifted by 6 months to facilitate the comparisons of the Northern and Southern Hemisphere data. At the South Pole the mesopause region is constantly illuminated by the Sun for more than 6 months in summer and is in complete darkness the rest of the year. While solar tides are present, their amplitudes are significantly weaker than at midlatitudes [*Forbes et al.*, 1995]. At 40°N the diurnal variation in solar illumination has a significant impact on photochemistry and generates strong tides which affect both the Fe and Na layers. *States and Gardner* [1999] showed that for Na the largest impact occurs on the bottomside of the layer where near 80 km the nighttime Na density is less than half the diurnal mean. Consequently, the nighttime layer is several hundred meters higher and several hundred meters

narrower than the diurnal mean layer. The Na harmonic fits at 40°N were obtained from data that were averaged over the complete diurnal cycle and so they are free of tidal affects and other diurnal biases [*States and Gardner*, 1999]. The Fe harmonic fits at 40°N were obtained from strictly nighttime observations [*Kane and Gardner*, 1993], which can lead to biases in the measured layer parameters similar to those observed in the Na measurements.

[10] At the South Pole the annual mean Fe abundance (all annual mean values are derived from the harmonic fits to avoid sampling biases) is about 8% smaller than the mean at 40°N, while the mean Na abundance is about 16% larger. These differences are not significant because lidar calibration errors could result in density and abundance errors of ±10%. The seasonal variations in Na abundance are significantly larger at the South Pole with the summer abundances almost 10 times smaller than at 40°N. The seasonal variations in all three layer parameters for both Fe and Na are larger at the South Pole, with the biggest differences in the centroid height variations. For both Fe and Na the annual variations in the centroid height are nearly a factor of 10 larger at the South Pole compared to 40°N. Furthermore, the semiannual variations in centroid height are smaller at the South Pole, especially for Na. In spite of these considerable differences, the annual mean values of the centroid heights at these two sites differ by only 450 m for Fe and 100 m for Na. On average, both layers are slightly higher at the South Pole. At 40°N the RMS width of the Na layer is dominated by a semiannual oscillation while at the South Pole, annual oscillations dominate. At the South Pole, the annual mean RMS layer width is about 23% larger for Fe and 25% smaller for Na compared with 40°N.

3. Seasonal Density Variations

[11] To determine the dominant harmonic components of the Fe and Na densities, at each altitude the 12-, 6-, 4-,

Figure 2. Weekly mean (a) Na column abundance, (b) Fe column abundance, (c) Na centroid height, (d) Fe centroid height, (e) Na layer RMS width, and (f) Fe layer RMS width at the South Pole. Fe data are marked as squares, and Na data are marked as triangles. The harmonic fits (mean + annual + semiannual) for Na and Fe data are plotted as solid curves. For comparison, the harmonic fits for observations made at the Urbana Atmospheric Observatory (40°N) are plotted as dashed curves [*Kane and Gardner*, 1993; *States and Gardner*, 1999]. The Urbana harmonic fits have been shifted by 6 months to facilitate the comparisons.

Table 1. Characteristics of Fe and Na Layers Observed at South Pole[a]

	Annual Mean A_o	Annual Amplitude A_1	Annual Phase B_1, days	Semiannual Amplitude A_2	Semiannual Phase B_2, days	Amplitude Ratio A_1/A_2	RMS Residual
Fe abundance ($\times 10^9$ cm^{-2})	9.7	6.2	175	0.6	156	9.9	4.7
Na abundance ($\times 10^9$ cm^{-2})	4.3	3.5	179	0.5	102	7.1	1.4
Fe centroid height, km	88.4	2.5	11	1.6	173	1.6	1.3
Na centroid height, km	91.5	2.2	−13	0.5	168	4.6	0.8
Fe RMS width, km	4.2	1.5	173	0.4	111	3.9	0.6
Na RMS width, km	3.7	1.8	177	0.1	93	17.4	0.3

[a]$A = A_o + A_1 \cos\left[\frac{2\pi}{365}(\text{day} - B_1)\right] + A_2 \cos\left[\frac{2\pi}{182.5}(\text{day} - B_2)\right]$.
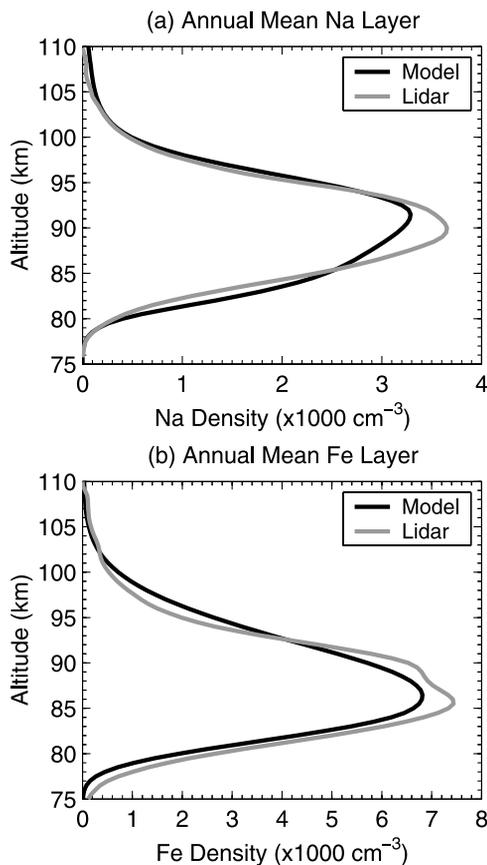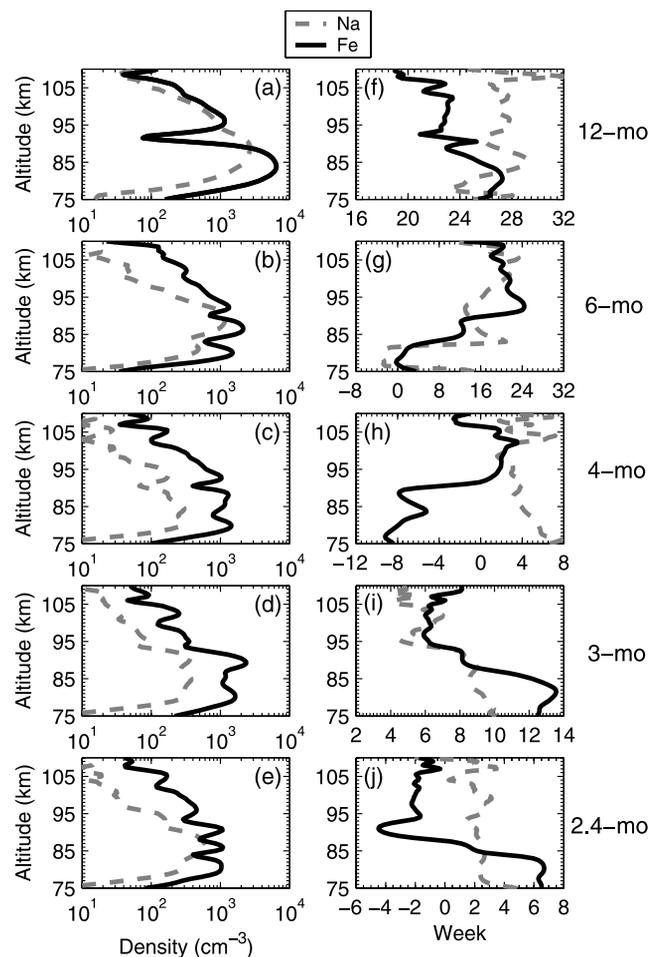
Figure 3. Comparison plots of the annual mean concentration profiles of (a) mesospheric Na and (b) Fe above the South Pole that were derived from lidar measurements and model calculations.

periods less than about 4 weeks and substantially reduces the amplitudes of fluctuations with periods of about 2 months or less. The data plotted in Figure 5 are also part of the UISP-02 South Pole observational model and can be accessed via the University of Illinois web site (http://conrad.csl.uiuc.edu/Research/SouthPole/).

[13] To help understand the temperature dependency of metallic layer structure, the UISP-02 temperatures from 75 to 110 km throughout the year are shown in Figure 6 [*Pan and Gardner*, 2003]. The extremely low Fe and Na densities below 90 km in midsummer correspond to the period and height range of coldest temperatures. Notice also that the Na layer exhibits local maxima in density near 90 km, immediately following the local temperature maxima that occur near the fall and spring equinoxes. The correlations between the measured temperatures and metal densities are plotted versus altitude in Figure 7. Below 90 km both species are highly correlated with temperature. In the lower thermo-

3-, and 2.4-month oscillations were fitted successively to the weekly mean density data sets plotted in Figure 1. The annual mean and harmonic amplitude profiles were smoothed by (1) applying parabolic fits to their logarithms, (2) subtracting the fits and smoothing the residuals with a 1-km FWHM Hamming window, and (3) then adding the smoothed residuals back to parabolic fits. The results are shown in Figure 3 for annual mean profiles (comparison with the modeled mean profiles in Figure 3 will be made in the next section), and in Figures 4a–4e for the amplitudes of each harmonic, along with their corresponding phases in Figures 4f–4j. Both layers show strong 12-month oscillations with amplitudes comparable to the annual mean density levels (Figure 3).

[12] To more completely characterize the seasonal variations of the Fe and Na layers, the weekly mean profiles plotted in Figure 1 were interpolated over gaps in the observations by first computing the mean plus annual and semiannual harmonic fits at each altitude between 75 and 110 km. The harmonic fits were subtracted from the weekly mean density profiles, and the residuals were smoothed by a Hamming window with a FWHM of 8 weeks and a resolution of 1 week. The smoothed residuals were then added back to the mean plus annual and semiannual fits, and the results are plotted versus month in Figures 5a and 5b. This approach eliminates temporal fluctuations with

Figure 4. Altitude profiles of the (a) 12-month amplitude, (b) 6-month amplitude, (c) 4-month amplitude, (d) 3-month amplitude, (e) 2.4-month amplitude, (f) 12-month phase, (g) 6-month phase, (h) 4-month phase, (i) 3-month phase, and (j) 2.4-month phase computed from the weekly mean Fe (solid curves) and Na (dashed curves) density profiles plotted in Figure 1.
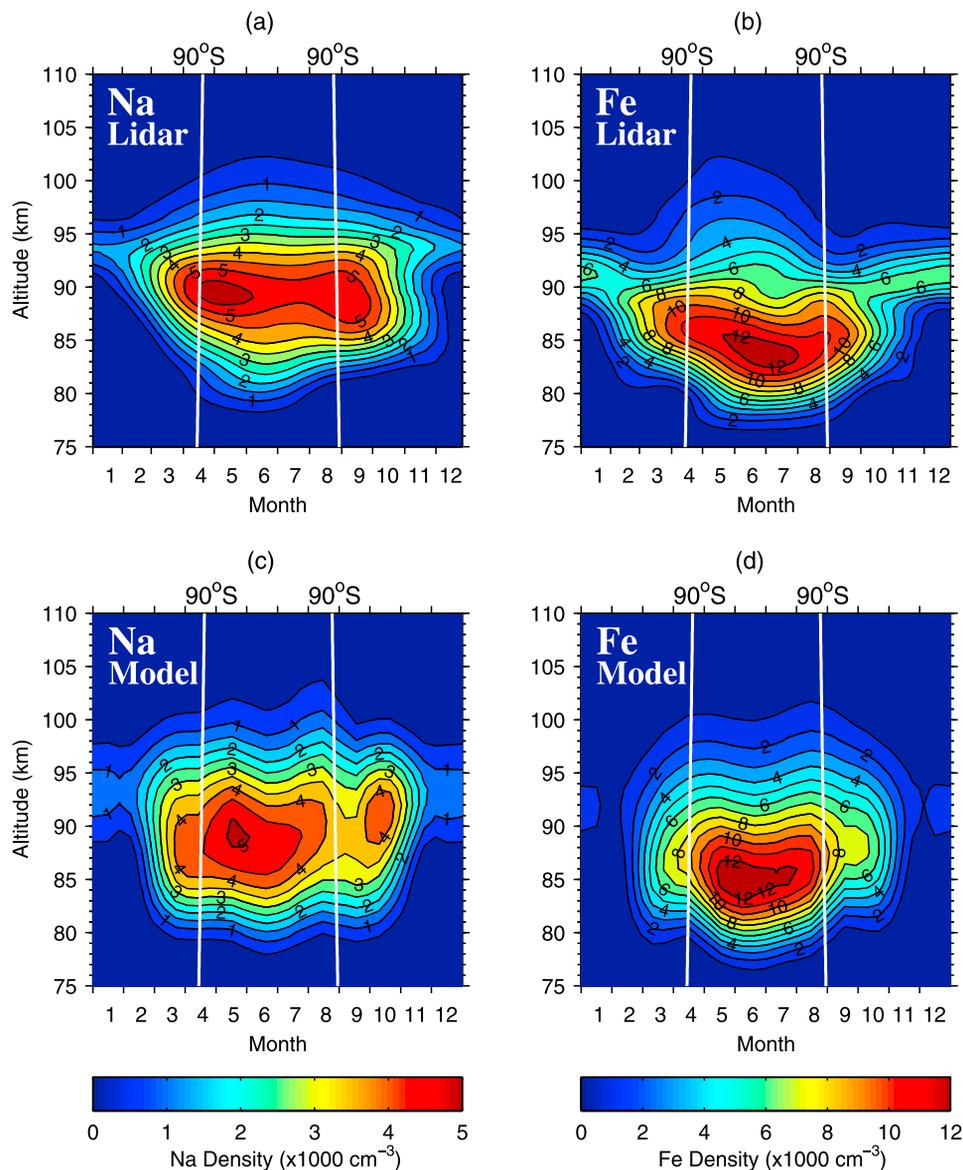
Figure 5. Observed and modeled weekly mean Na and Fe density profiles at the South Pole. Polar night (24 hours of darkness) occurs between the white curves. (a, b) The measured densities, from the UISP-02 observational model, and (c, d) the modeled densities.

sphere region, both species exhibit negative correlation with temperature.

4. Modeling the Fe and Na Layers

4.1. Model Description

[14] In order to model the seasonal behavior of the metal layers at the South Pole, we employ a new time-resolved model of metal species in the mesosphere/lower thermosphere [*Plane*, 2004]. Figure 8 shows schematically the design of the model. The input data (temperature, winds, minor species, etc.) are provided from both observations (e.g., lidar) and a variety of models (e.g., global circulation models and empirical models). A mesospheric model with fine vertical resolution (MESOMOD) is then used to produce a consistent set of concentration profiles for the background neutral species (O_3, O_2, O, H, H_2, H_2O, and CO_2) that control the chemistry of the metal layers. These

data, together with physical transport parameters, are then input into the models of sodium and iron, termed NaMOD and FeMOD, respectively.

[15] In NaMOD, the concentrations of the three major gas-phase sodium species, Na, $NaHCO_3$, and Na^+, are determined by full solution of their respective continuity equations. These equations include terms for production of these species by meteoric ablation, and removal by uptake on meteor smoke and polar mesospheric cloud particles (these processes are discussed further below). Other sodium species, such as NaO, NaOH, and Na^+ cluster ions, are short-lived intermediates and are therefore treated in chemical steady state. NaMOD is one dimensional, extending from 65 to 110 km with a height resolution of 0.5 km. The continuity equations are integrated with a 10-min time step using a time-implicit integration scheme [*Shimazaki*, 1985]. The background mesospheric species that control the sodium chemistry are read in every 20 model minutes.
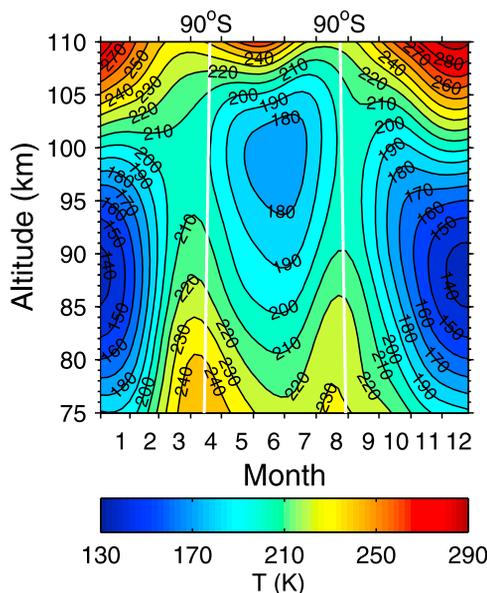
Figure 6. Observed weekly mean temperatures between 75 and 110 km at the South Pole derived from the UISP-02 climatology [*Pan and Gardner*, 2003].

In FeMOD, the major species Fe, FeOH, and Fe^+ are determined by full solution of their respective continuity equations, and all other iron species are considered to be in steady state. The gas-phase reactions of sodium and
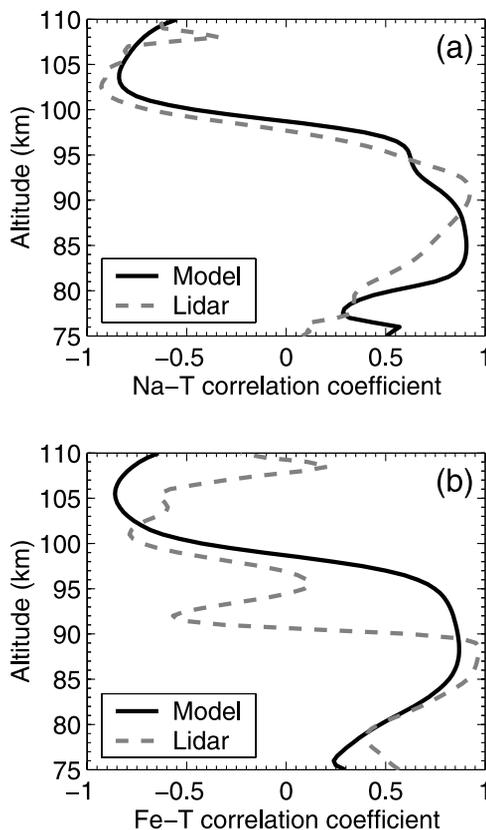
Figure 7. Correlation coefficients between the measured and modeled metal densities and temperature above the South Pole plotted from 75 to 110 km. (a) Na-temperature correlation and (b) Fe-temperature correlation.
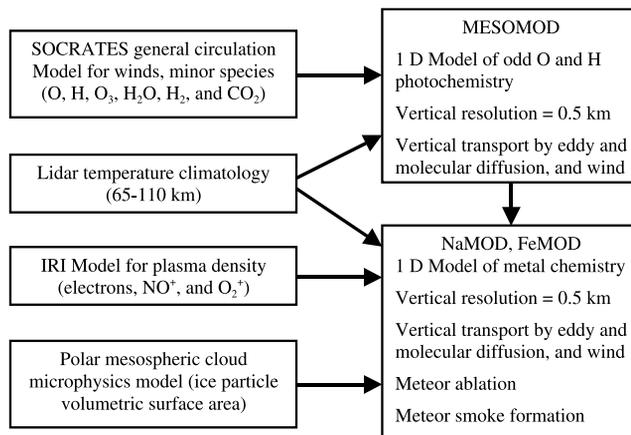
Figure 8. Schematic diagram of the mesospheric Na and Fe chemical/dynamical models.

iron, and their rate coefficients, are taken from recent compilations [*Plane*, 2002; *Plane et al.*, 2003; *Plane*, 2004].

[16] The transport of the metal constituents is assumed to be governed by the same eddy diffusion coefficient K_{zz} up to the turbopause at about 100 km, and above this height by molecular diffusion. Vertical transport by the net vertical wind, w, which arises from the pronounced meridional circulation in the upper mesosphere, is also included. K_{zz} and w are calculated using the NCAR interactive two-dimensional global circulation model SOCRATES [*Khosravi et al.*, 2002]. The temperature profile between 65 and 110 km is taken from the UISP-02 observational climatology [*Pan and Gardner*, 2003]. The runs of NaMOD and FeMOD shown here were integrated for 20 model days to ensure that the diurnal behavior of the metal layer had stabilized.

[17] MESOMOD is also one-dimensional, extending from 65 to 110 km with a height resolution of 0.5 km. It contains a full treatment of the odd oxygen and hydrogen chemistry in the MLT, with rate coefficients taken from the NASA/JPL compilation [*DeMore et al.*, 1997]. K_{zz} and w are again input from SOCRATES, and this model also supplies the H_2O, H_2, and CO_2 mixing ratios at the lower boundary (65 km). Diurnally averaged values for all these parameters were used. Note that SOCRATES does not include tides explicitly; however, this should not be important in this paper since we are comparing 7-day averaged data. Parameterized codes for the photolysis of O_3, H_2O, HO_2, H_2O_2, and O_2 at Lyman-α and in the Schumann-Runge continuum are used [*Brasseur and Solomon*, 1998; *Shimazaki*, 1985]. The photolysis of O_2 in the Schumann-Runge bands is calculated using a recent formalism [*Koppers and Murtagh*, 1996]. MESOMOD uses time-implicit integration with a 2-min time step, and was run for 5 model days before a set of diurnal concentration profiles was recorded every 20 min for input into NaMOD or FeMOD. Note that because the concentration of the sodium or iron species is at least 4 orders of magnitude less than species such as O_3 or H in the MLT, the background chemistry is essentially decoupled from the metals. Profiles of NO^+, O_2^+ and e^- are input for the appropriate year and time-of-

day from the International Reference Ionosphere 2000 model [*Bilitza*, 2003].

4.2. Meteoric Input

[18]   The physics of meteoroid ablation has been treated in detail by several investigators [e.g., *Hunten et al.*, 1980; *Love and Brownlee*, 1991]. The problem becomes reasonably tractable for particles less than about 250 μm in radius, because heat conductivity through the particle is fast enough for the particle to be treated as isothermal. The analysis of small particle impact craters on the Long Duration Exposure Facility (LDEF), an orbital impact detector placed on a spacecraft for several years, shows that most of the total mass of cosmic dust is made up from particles smaller than this [*Love and Brownlee*, 1993], thereby justifying the neglect of heat conductivity. The frictional heating of the meteoroid by collisions with air molecules is balanced by radiative losses, and by the absorption of heat energy through temperature increases, melting, phase transitions, and vaporization [e.g., *Plane*, 2004].

[19]   Assuming that most of the extra-terrestrial material has the composition of ordinary chondrites, with an abundance (by mass) of 0.6% and 11.5% for Na and Fe, respectively [*Mason*, 1971], then these elements might be expected to ablate in a molar ratio of 1:7.9. However, a more realistic approach involving differential ablation has been proposed [*McNeil et al.*, 1998], with the relatively volatile elements such as Na and K evaporating first and refractory elements evaporating last. The differential ablation model used here contains the following treatment, based on a planetary fractionation model [*Fegley and Cameron*, 1987]. When the meteoroid temperature reaches 1200 K, further frictional heat input to the particle is balanced by vaporization and radiative cooling, and no further temperature rise occurs until the initial 20% of the meteoroid mass has evaporated. All of the Na is assumed to evaporate in the first 5% of this fraction. Evaporation then ceases until the temperature reaches 2100 K, when 78% of the mass evaporates. The final 2%, containing the most refractory elements (e.g., Ca), then evaporates if the temperature reaches 2500 K.

[20]   When this model is used to integrate over the meteoroid mass and velocity distribution estimated from the LDEF experiment [*McBride et al.*, 1999], about 62% of the total incoming material is predicted to vaporize. Na and Fe ablate in the ratio 1:3.5, with the peak ablation rates at 92 and 88 km, respectively. These heights are in sensible accord with recent meteor radar measurements at the South Pole, which reported peak echoes between 91 and 93 km [*Janches et al.*, 2004]. The ablation model assumes a seasonally constant entry angle of 37° to zenith; future meteor radar observations at the South Pole should enable this assumption to be refined [*Janches et al.*, 2004]. In the NaMOD and FeMOD models, the ablation profiles are then modulated with a diurnal and seasonal variation taken from a recent radio meteor survey [*Yrjola and Jenniskens*, 1998].

4.3. Heterogeneous Removal of Metallic Species on Smoke and Ice Particles

[21]   Removal of the gas-phase metallic species is modeled by heterogeneous uptake on meteoric smoke particles or PMC ice particles. Meteor smoke has been proposed to form through the recondensation of vaporized meteoroids [*Hunten*

et al., 1980]. The vertical profile of the volumetric surface area of meteor smoke is calculated here using a one-dimensional model which includes meteoric ablation, polymerization of metal-containing molecules [*Plane*, 2004], growth by condensation and coagulation [*Jacobson et al.*, 1994], and sedimentation. The model shows that the meteor smoke particles do not grow large enough (>2 nm) to sediment rapidly (the particles would take about 45 days to sediment to below 60 km) [*Gabrielli et al.*, 2004]. We assume that all the vaporized meteoroid constituents, including silicon, form oxides or hydroxides that are condensable (note that a 2-nm particle would contain about 200 $FeSiO_3$ molecules).

[22]   The uptake of sodium and iron species on these smoke particles is likely to be highly efficient, and an uptake coefficient of 1.0 is assumed in NaMOD and FeMOD. This is consistent with recent laboratory experiments using the fast flow tube technique [*Murray and Plane*, 2003], where we have shown that both Na and Fe atoms stick with very high efficiency on a silica surface (B. J. Murray and J. M. C. Plane, unpublished results, 2004). Molecules such as $NaHCO_3$ and FeOH, which have large dipole moments, should also stick with high probability. *Plane* [2004] has shown that the uptake of $NaHCO_3$ on meteor smoke is an essential removal process to explain the absence of a diurnal variation in the column abundance of the Na layer at midlatitudes [*States and Gardner*, 1999].

[23]   To calculate the uptake of the metallic species in a PMC, we start with the vertical profile of ice particle size distribution predicted from a recent cloud microphysics model [*Berger and von Zahn*, 2002]. We have previously adapted this profile to model the Fe layer at the South Pole in the presence of a typical strong PMC (on 19 January 2000), where complete removal of Fe atoms was observed inside the cloud [*Plane et al.*, 2004]. In order to match the observed Mie scattering brightness of this cloud at 374 nm, the number density of ice particles was reduced by 10% at all heights, and a vertical height shift was applied to the particle number and size distributions [*Plane et al.*, 2004]. This takes account of the strong upwelling over Antarctica during the austral summer, which causes the cloud layers to be about 2 km higher at the South Pole compared to northern high latitudes [*Gardner et al.*, 2001; *Chu et al.*, 2003]. The shift applied was a constant 2.4 km up to 85.5 km, decreasing with a scale height of 3 km at higher altitudes. This scale height gives the best fit to the observation, and is in accord with the decrease in w by about an order of magnitude between 85 and 95 km, predicted by GCMs such as SOCRATES. The volumetric surface area of the PMC is plotted in Figure 9. Note that although the maximum surface area peaks around 85.5 km, there is still a significant ice surface area at heights well above where the cloud is visible by lidar, because of a large density of small particles with radii smaller than 15 nm.

[24]   We have also shown in the laboratory that the uptake coefficients of Na and Fe atoms on cubic-crystalline ice are essentially unity over the relevant temperature range of 130 to 150 K (B. J. Murray and J. M. C. Plane, unpublished results, 2004). Once again, metallic ions and polar species such as $NaHCO_3$ and FeOH should exhibit highly efficient uptake on H_2O-ice surfaces. We therefore assume in NaMOD and FeMOD that the uptake coefficient is unity for all metallic species. The lidar observations, which are made in
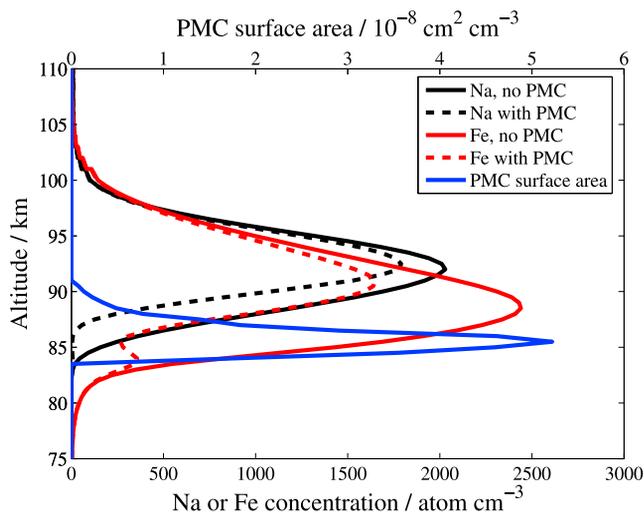
Figure 9. Modeled profiles of the Na and Fe layers at the South Pole during January, in the presence and absence of PMC. The profile of PMC volumetric surface area shown is for a typical individual cloud [*Plane et al.*, 2004]. The monthly average PMC surface area during January is about 25% of this value.

the Eulerian reference frame, provide a measure of PMC brightness and occurrence frequency. During midsummer at the South Pole (i.e., December–January), strong PMC are seen for only about 10% of the observing time, whereas weaker PMC are visible for 67% [*Chu et al.*, 2003]. However, converting these data into an estimate of the weekly averaged PMC surface area for the model is complicated by the time-scales of the various processes involved: cloud formation, sedimentation, transport, and decay. We therefore assume that the average PMC surface area profile during December and January is 25% of the strong PMC surface area illustrated in Figure 9, and that this drops to 5% by early November or late February. This parameterization is crude but probably adequate for the purpose of investigating the seasonal variability of the metal layers.

[25] The formation of a strong PMC almost certainly causes a significant redistribution of water vapor in the high-latitude summer mesosphere: dehydration of the region between about 97 and 92 km (for the South Pole), and the humidification of the region immediately below [*von Zahn and Berger*, 2003]. While this affects the odd O and H chemistry [*Murray and Plane*, 2004], the impact on the metal layers is small (according to the model) because a substantial fraction of the metals in this height range are removed by uptake on the ice particles whose formation has caused the dehydration. Bearing in mind that strong PMCs are present for a relatively small fraction of the time (see above), we have not included the redistribution of H_2O by PMC formation when calculating the weekly averaged profiles of H_2O, and the odd O and H species, in MESOMOD.

5. Modeling Results and Discussion

5.1. Metal Input and Heterogeneous Removal

[26] The best fit of NaMOD and FeMOD to the lidar measurements between September and April (i.e., excluding the winter months; see below), is obtained with the average

input fluxes from ablation of Na and Fe set to 9.6×10^3 and 3.4×10^4 atom $cm^{-2} s^{-1}$, respectively. This Na input flux is at the upper end of the range estimated by *Plane* [2004], and is a consequence of the larger K_{zz} values calculated by SOCRATES (the average K_{zz} between 80 and 90 km ranges from $4.2-10.7 \times 10^5 cm^2 s^{-1}$ over these months of the year). These fluxes are equivalent to a global mass ablation rate of 27.0 t d^{-1}. Although this mass ablation rate is in accord with a very recent estimate of 38 ± 14 t d^{-1} which was obtained by measuring the accumulation of iridium and platinum in a Greenland ice core over the Holocene [*Gabrielli et al.*, 2004], it is a sensitive function of K_{zz} between 80 and 90 km [*Plane*, 2004]. Unfortunately, this parameterization of vertical diffusive transport is rather uncertain. For instance, measurements of turbulent energy dissipation rates at high (northern) latitudes [*Lübken*, 1997] indicate that K_{zz} could be a factor of 2 higher during summer, compared with the SOCRATES prediction. This would then require a mass ablation rate of around 60 t d^{-1} to model the observed Na and Fe layers.

[27] Figure 9 demonstrates the effect of heterogeneous removal of the metals on ice particles during January, by showing the modeled profiles of Na and Fe with and without uptake on PMC. The removal of metal atoms is more pronounced on the underside of the Fe layer, because this layer occurs about 5 km lower than the Na layer and therefore overlaps more closely with the PMC at 85.5 km. In contrast to our recent study showing complete removal of Fe inside a strong PMC [*Plane et al.*, 2004], the volumetric surface area of PMC averaged over January is only about 25% of that in the strong PMC illustrated in Figure 9 (see above), so that there is incomplete removal of Fe at the peak of the PMC. Note that the PMC depletes the metal layers even above 90 km where there are no ice particles. This is because heterogeneous removal below 90 km results in increased downward diffusion of the metals.

5.2. Wintertime Layers

[28] Modeling the Na and Fe layers at the South Pole during winter leads to two interesting conclusions. The first concerns the velocity of the net vertical wind, w. During winter, there should be strong downward transport into the polar vortex. For example, SOCRATES predicts that w should be about -3.2 cm s^{-1} between 75 and 85 km during June. However, this large velocity causes the ledges of atomic O and H to be pushed down to around 75 km. Since the undersides of the metal layers are controlled by the fall-off of these species (because they reduce the metal reservoirs such as FeOH and $NaHCO_3$ back to atomic Fe and Na), the peak heights of the Fe and Na layers would also be pushed down to 74 and 77 km, respectively, as shown in Figure 10. However, the observed peak heights are actually about 84 and 87 km, i.e., 10 km higher. By reducing w to -0.8 cm s^{-1} between 75 and 85 km (i.e., 25% of the value in SOCRATES), satisfactory agreement is achieved between the modeled and observed layers (Figure 10). Note that in contrast to w, the metal layer heights are not particularly sensitive to K_{zz} [*Plane*, 2004, Figure 6].

[29] This exercise illustrates that the metal layers at high latitudes during winter are a rather sensitive tracer of net vertical motion. Additional confirmation that w is too high in SOCRATES is that the associated adiabatic heating leads
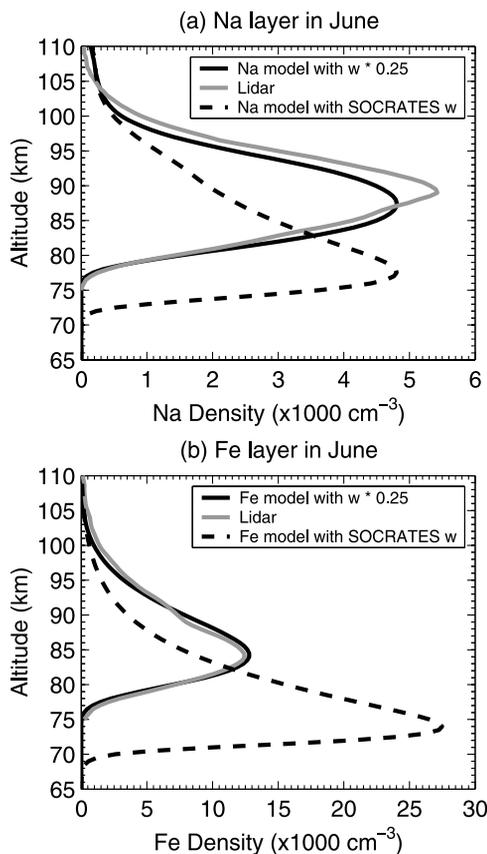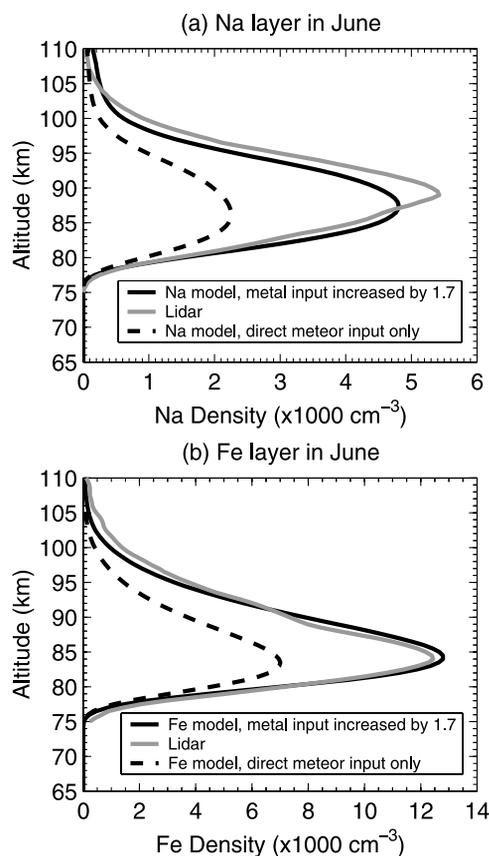
Figure 10. Comparison of the observed and modeled (a) Na and (b) Fe layers in June. The predicted vertical wind, w, from the SOCRATES global circulation model is too large (w = −3.2 cm/s between 75 and 85 km), causing the layers to be displaced downward by about 10 km. Reduction of w by a factor of 0.25 produces good agreement with the observations.

to winter temperatures in the upper mesosphere that are significantly too warm; for example, SOCRATES predicts 265 K during June at 75 km, compared with the UISP-02 observations of 226 K (see Figure 6). Note that a similar discrepancy has been noted during winter with the three-dimensional TIME-GCM [*Pan et al.*, 2002]. In the model results described below, the SOCRATES w was multiplied by a factor of 0.25 before being input into MESOMOD, NaMOD, and FeMOD for all months of the year, although this only has a significant effect on the metal layers between May and August.

[30] The second conclusion to be drawn when modeling the winter layers is that there has to be an additional input of gas-phase metallic species, apart from direct meteoric ablation. This is demonstrated in Figure 11, which compares the modeled and observed Na and Fe layers during June. In order to model the observations satisfactorily, the input from meteoric ablation needs to be increased by a factor of 1.7 (Figure 11). In fact, this factor may be an underestimate if the results of a recent report of meteor radar rates at the South Pole [*Janches et al.*, 2004], showing that the winter-time meteor rate is about half the yearly average rate, are confirmed by longer-term measurements. The most likely source of additional metals is the convergence over the Pole

of air transported from lower latitudes by the meridional wind. This air will contain several days of meteoric input (the average lifetime of the metals above 80 km is about 1 week). The mixing ratio of gas-phase metals increases from 85 to 105 km in order to sustain a net downward flux that balances ablation. Thus when air above 90 km converges and descends, this should lead to an increase in the concentration of the metal atom layers. A detailed model of the convergence process is beyond the scope of this paper, although this would make a very useful test of transport in GCMs, at high latitudes in the MLT. Here we simply increase the metal input by a factor of 1.7, between May and August.

[31] From the recent measurements of cosmic Ir and Pt in a Greenland ice core [*Gabrielli et al.*, 2004] it was estimated that the rate of deposition into the troposphere of meteoric material during winter at high latitudes is about a factor of 10 higher than the annual average global meteoric input rate. However, much of this material is transported to the winter polar region from the entire mesosphere above 60 km, and so the ablation products will mostly have formed meteoric smoke long before reaching the South Pole, and no longer act as a reservoir for the metal atom layers. This is consistent with the smaller factor of 1.7 that we apply here to enhance the

Figure 11. Comparison of the observed and modeled (a) Na and (b) Fe layers in June, showing that the input of the metals needs to be increased by a factor of 1.7 over the direct meteoric ablation rate. This most likely arises from the wintertime convergence of the meridional wind over the South Pole, with descent of air from above 90 km.
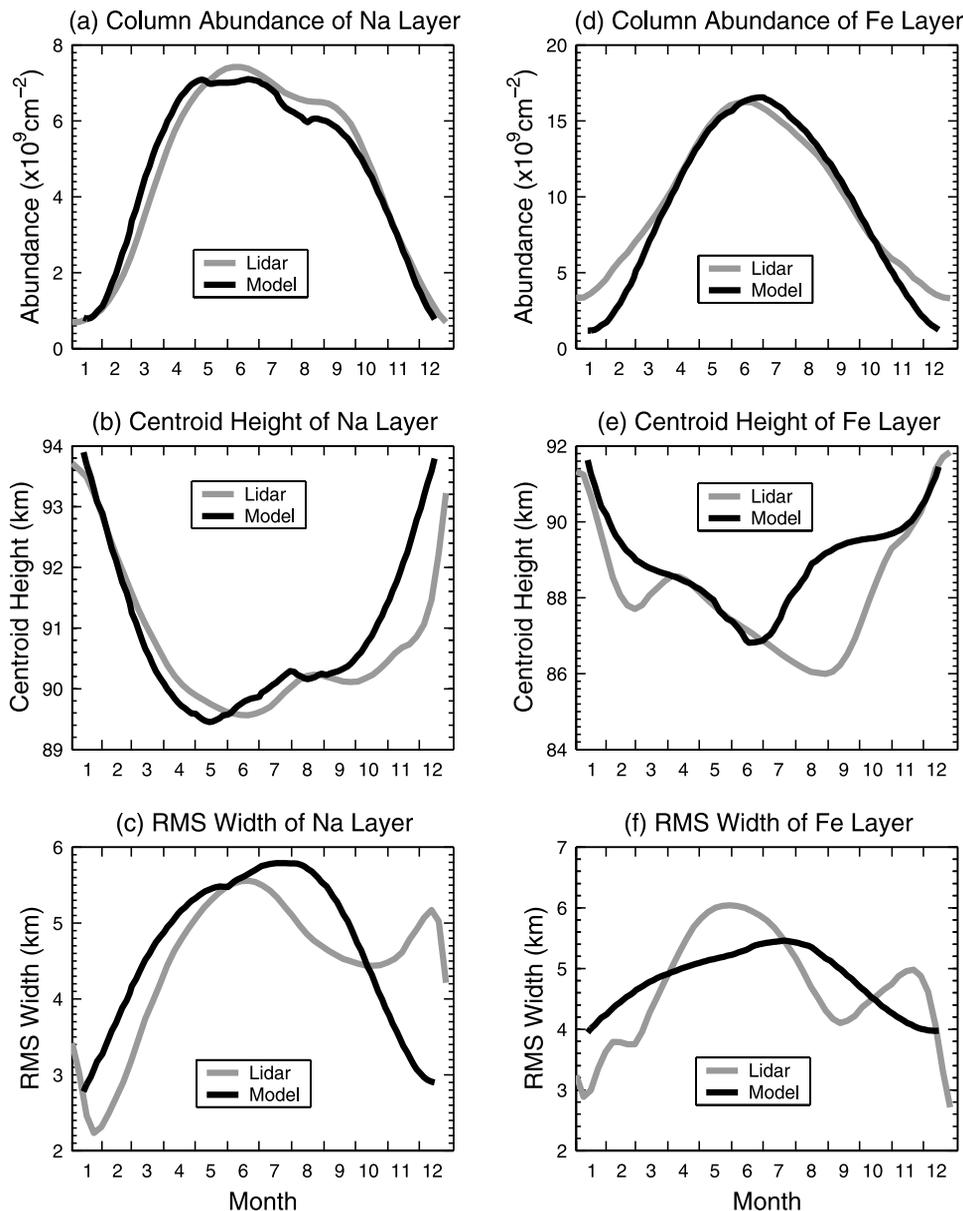
Figure 12. The weekly mean (a) Na layer column abundance, (b) Na layer centroid height, (c) Na layer RMS width, (d) Fe layer column abundance, (e) Fe layer centroid height, and (f) Fe layer RMS width at the South Pole plotted versus month. The observed and modeled curves were derived from the concentration profiles plotted in Figure 5.

wintertime Na and Fe input from ablation occurring only relatively close to the South Pole.

5.3. Seasonal Variability of the Layers

[32] We now compare the observed seasonal behavior of the Na and Fe layers with the predictions of the model described in the previous section, including the modifications to the vertical velocity w and the wintertime input of the metals as described above. Figure 3 shows that the annual average Na and Fe layers are modeled satisfactorily. The good agreement of the top and bottom scale heights, and the peak heights of the layers, is evidence that the ion-molecule chemistry that controls the topsides of the layers, and the neutral chemistry that governs the undersides, are well described in NaMOD and FeMOD.

[33] The correlation plots in Figure 7 between the Na and Fe densities and temperature also show good agreement between the lidar observations and the model, particularly for Na. The negative correlation coefficients above 97 km result from ion-molecule cluster reactions of Na^+ and Fe^+ [*Plane*, 2004; *Plane et al.*, 2003]. The resulting clusters then undergo dissociative recombination with electrons, forming Na and Fe. Because these reactions become faster at lower temperature, the balance between the metal ions and atoms shifts to the atoms at lower temperatures. The positive correlation coefficients below 95 km arise from three factors. First, the reactions that convert the neutral reservoirs such as FeOH and $NaHCO_3$ back to Fe and Na have significant activation energies [*Plane*, 2004; *Plane et al.*, 2003], so that the balance moves toward the metal atoms at

higher temperatures. Second, PMCs form at temperatures below about 150 K, and these remove a significant fraction of the neutral constituents below 95 km (Figure 9). Third, in winter the convergence of the meridional wind and resulting descent of metallic species from above 90 km causes both an increase in temperature and metal atom concentration.

[34] Figure 5 compares contour plots of the observed and modeled seasonal variations of the Na and Fe layers. The abrupt and substantial disappearance of Na and Fe below 90 km when PMCs form in summer (mid-November to mid-February) is captured well by the model. The Na layer exhibits two maxima, in late April and in September, which are replicated well. The single maximum in the Fe layer appears a month earlier in the model compared with the observations, although the height and absolute concentration are satisfactory. Finally, the observed and modeled column abundances, centroid heights, and RMS widths of the Na and Fe layers are compared as a function of month in Figure 12. In all cases, but especially for the column abundances and centroid heights, which exhibit large seasonal changes at the South Pole, the model satisfactorily reproduces the observed variations of these parameters.

6. Conclusions

[35] The annual mean profiles of the mesospheric Na and Fe layers at the South Pole are remarkably similar to those observed at lower latitudes in the Northern Hemisphere. The annual mean abundances for both species are virtually identical to midlatitude values, within the calibration accuracy of the lidar measurements ($\pm 10\%$). The annual mean centroid height is just 100 m higher for Na and 450 m higher for Fe compared to $40°N$. The most striking feature of the seasonal changes in the metal layer profiles at the South Pole is the almost complete absence of Na and Fe below 90 km during midsummer. This leads to significantly higher metal layers with narrower widths and smaller abundances than are observed at lower latitudes during the summer. The seasonal variations in the Na and Fe layer centroid heights are nearly a factor of 10 larger at the South Pole compared to $40°N$. In addition, the seasonal variations in Na abundance are significantly larger with the summer abundances almost 10 times smaller at the South Pole than at $40°N$.

[36] The models that we have constructed reproduce most features of the observations very well. The gas-phase chemistry of sodium and iron is derived from laboratory studies of some 40 individual chemical reactions under conditions appropriate to the MLT [*Plane*, 2002, 2003], and appears to provide a satisfactory description of the kinetics for interconverting Na and Fe atoms into various reservoir species. This study also demonstrates the importance of the rapid uptake of the metallic species on both ice (PMCs) and meteoric smoke particle surfaces. However, it must be emphasized that the model contains two important empirical corrections, which emerge from comparison with the observations. First, the downward vertical velocity in winter must be less than about 1 cm s^{-1} in the upper mesosphere, in order to avoid displacing the minor constituents O, H, and the metal layers too far below 85 km. Second, the required additional input of metallic species during the winter months appears to arise from the winter-

time convergence of the meridional flow over the South Pole. These are two examples where observations of the metal layers provide a sensitive test of the large-scale dynamics of the upper atmosphere.

References

Alpers, M., J. Höffner, and U. von Zahn (1990), Iron atom densities in the polar mesosphere from lidar observations, *Geophys. Res. Lett.*, *17*, 2345–2346.
Avaste, O. (1993), Noctilucent clouds, *J. Atmos. Terr. Phys.*, *55*, 133–143.
Berger, U., and U. von Zahn (2002), Icy particles in the summer mesopause region: Three-dimensional modeling of their environment and two-dimensional modeling of their transport, *J. Geophys. Res.*, *107*(A11), 1366, doi:10.1029/2001JA000316.
Bilitza, D. (2003), International Reference Ionosphere 2000: Examples of improvements and new features, *Adv. Space Res.*, *31*, 757–767.
Bowman, M. R., A. J. Gibson, and M. C. W. Sandford (1969), Atmospheric sodium measured by a tuned laser radar, *Nature*, *221*, 456–457.
Brasseur, G., and S. Solomon (1998), *Aeronomy of the Middle Atmosphere*, Springer, New York.
Chu, X., G. Papen, W. Pan, C. S. Gardner, and J. Gelbwachs (2002), Fe Boltzmann temperature lidar: Design, error analysis, and first results from the North and South poles, *Appl. Opt.*, *41*, 4400–4410.
Chu, X., C. S. Gardner, and R. G. Roble (2003), Lidar studies of interannual, seasonal, and diurnal variations of polar mesospheric clouds at the South Pole, *J. Geophys. Res.*, *108*(D8), 8447, doi:10.1029/2002JD002524.
Collins, R. L., and R. W. Smith (2004), Evidence of damping and overturning of gravity waves in the Arctic mesosphere: Na lidar and OH temperature observations, *J. Atmos. Sol. Terr. Phys.*, *66*, 867–879.
Collins, R. L., A. Nomura, and C. S. Gardner (1994), Gravity waves in the upper mesosphere over Antarctica: Lidar observations at the South Pole and Syowa, *J. Geophys. Res.*, *99*, 5475–5485.
DeMore, W. B., S. P. Sander, D. M. Golden, R. F. Hampson, M. J. Kurylo, C. J. Howard, A. R. Ravishankara, C. E. Kolb, and M. J. Molina (1997), Chemical kinetics and photochemical data for use in stratospheric modeling, in *Evaluation 12*, JPL Publ., *97–4*, 278 pp.
Fegley, J. B., and A. G. W. Cameron (1987), Vaporization model for iron/silicate fractionation in the Mercury protoplanet, *Earth Planet. Sci. Lett.*, *82*, 207–222.
Forbes, J. M., N. A. Makarov, and Y. I. Portnyagin (1995), First results from the meteor radar at South Pole: A large 12–hour oscillation with zonal wave number one, *Geophys. Res. Lett.*, *22*, 3247–3250.
Gabrielli, P., et al. (2004), Meteoric smoke fallout over the Holocene revealed by iridium and platinum in Greenland ice, *Nature*, *432*, 1011–1014.
Gardner, C. S., D. C. Senft, and K. H. Kwon (1988), Lidar observations of substantial sodium depletion in the summertime Arctic mesosphere, *Nature*, *332*, 142–144.
Gardner, C. S., G. C. Papen, X. Chu, and W. Pan (2001), First lidar observations of middle atmosphere temperatures, Fe densities, and polar mesospheric clouds over the North and South poles, *Geophys. Res. Lett.*, *28*, 1199–1202.
Gelbwachs, J. A. (1994), Iron Boltzmann factor lidar: Proposed new remotesensing technique for mesospheric temperature, *Appl. Opt.*, *33*, 7151–7156.
Granier, C., J. P. Jegou, and G. Megie (1989), Iron atoms and metallic species in the Earth's upper atmosphere, *Geophys. Res. Lett.*, *16*, 243–246.
Helmer, M., J. M. C. Plane, J. Qian, and C. S. Gardner (1998), A model of meteoric iron in the upper atmosphere, *Geophys. Res. Lett.*, *103*, 10,913–10,925.
Hunten, D. M., R. P. Turco, and O. B. Toon (1980), Smoke and dust particles of meteoric origin in the mesosphere and stratosphere, *J. Atmos. Sci.*, *37*, 1342–1357.
Jacobson, M. Z., R. Lu, E. J. Jensen, and O. B. Toon (1994), Modeling coagulation among particles of different composition and size, *Atmos. Environ.*, *28*, 1327–1338.
Janches, D., S. E. Palo, E. M. Lau, S. K. Avery, J. P. Avery, S. de la Pena, and N. A. Makarov (2004), Diurnal and seasonal variability of the me-

teoric flux at the South Pole measured with radars, *Geophys. Res. Lett.*, *31*, L20807, doi:10.1029/2004GL021104.

Kane, T. J., and C. S. Gardner (1993), Structure and seasonal variability of the nighttime mesospheric Fe layer at midlatitudes, *J. Geophys. Res.*, *98*, 16,875–16,886.

Kawahara, T. D., T. Kitahara, F. Kobayashi, Y. Saito, A. Nomura, C. Y. She, and D. A. Krueger (2002), Wintertime mesopause temperatures observed by lidar measurements over Syowa Station (69°S, 39°E), Antarctica, *Geophys. Res. Lett.*, *29*(15), 1709, doi:10.1029/2002GL015244.

Kawahara, T. D., C. S. Gardner, and A. Nomura (2004), Observed temperature structure of the atmosphere above Syowa Station, Antarctica (69°S, 39°E), *J. Geophys. Res.*, *109*, D12103, doi:10.1029/2003JD003918.

Khosravi, R., G. Brasseur, A. Smith, D. Rusch, S. Walters, S. Chabrillat, and G. Kockarts (2002), Response of the mesosphere to human-induced perturbations and solar variability calculated by a 2–D model, *J. Geophys. Res.*, *107*(D18), 4358, doi:10.1029/2001JD001235.

Koppers, G. A. A., and D. P. Murtagh (1996), Model studies of the influence of O$_2$ photodissociation parameterizations in the Schumann-Runge bands on ozone related photolysis in the upper atmosphere, *Ann. Geophys.*, *14*(1), 68–79.

Kurzawa, H., and U. von Zahn (1990), Sodium density and atmospheric temperature in the mesopause region in polar summer, *J. Atmos. Terr. Phys.*, *52*, 981–993.

Love, S. G., and D. E. Brownlee (1991), Heating and thermal transformation of micrometeoroids entering the Earth's atmosphere, *Icarus*, *89*, 26–43.

Love, S. G., and D. E. Brownlee (1993), A direct measurement of the terrestrial mass accretion rate of cosmic dust, *Science*, *262*, 550–553.

Lübken, F. J. (1997), Seasonal variation of turbulent energy dissipation rates at high latitudes as determined by in situ measurements of neutral density fluctuations, *J. Geophys. Res.*, *102*, 13,441–13,455.

Lübken, F. J., and J. Höffner (2004), Experimental evidence for ice particle interaction with metal atoms at the high latitude summer mesopause region, *Geophys. Res. Lett.*, *31*, L08103, doi:10.1029/2004GL019586.

Mason, B. (1971), *Handbook of Elemental Abundances of the Elements in Meteorites*, Gordon and Breach, New York.

McBride, N., S. F. Green, and J. A. M. McDonnell (1999), Meteoroids and small sized debris in low Earth orbit and at 1 au: Results of recent modeling, *Adv. Space Res.*, *23*, 73–82.

McNeil, W. J., E. Murad, and S. T. Lai (1995), Comprehensive model for the atmospheric sodium layer, *J. Geophys. Res.*, *100*, 16,847–16,855.

McNeil, W. J., S. T. Lai, and E. Murad (1998), Differential ablation of cosmic dust and implications for the relative abundances of atmospheric metals, *J. Geophys. Res.*, *103*, 10,899–10,911.

Megie, G., and J. E. Blamont (1977), Laser sounding of atmospheric sodium: Interpretation in terms of global atmospheric parameters, *Planet. Space Sci.*, *25*, 1093–1109.

Murray, B. J., and J. M. C. Plane (2003), The uptake of atomic oxygen on ice films: Implications for noctilucent clouds, *Phys. Chem. Chem. Phys.*, *5*, 4129–4138.

Murray, B. J., and J. M. C. Plane (2004), Modeling the impact of noctilucent cloud formation on atomic oxygen and other minor constituents of the summer mesosphere, *Atmos. Chem. Phys. Disc.*, *4*, 7181–7216.

Nomura, A., T. Kano, Y. Iwasaka, H. Fukunishi, T. Hirasawa, and S. Kawaguchi (1987), Lidar observations of the mesospheric sodium layer at Syowa Station, *Geophys. Res. Lett.*, *14*, 700–703.

Pan, W., and C. S. Gardner (2003), Seasonal variations of the atmospheric temperature structure at South Pole, *J. Geophys. Res.*, *108*(D18), 4564, doi:10.1029/2002JD003217.

Pan, W., C. S. Gardner, and R. G. Roble (2002), The temperature structure of the winter atmosphere at South Pole, *Geophys. Res. Lett.*, *29*(16), 1802, doi:10.1029/2002GL015288.

Plane, J. M. C. (2002), Laboratory studies of meteoric metal chemistry, in *Meteors in the Earth's Atmosphere*, edited by E. Murad and I. P. Williams, pp. 289–309, Cambridge Univ. Press, New York.

Plane, J. M. C. (2003), Atmospheric chemistry of meteoric metals, *Chem. Rev.*, *103*(12), 4963–4984.

Plane, J. M. C. (2004), A time-resolved model of the mesospheric Na layer: Constraints on the meteor input function, *Atmos. Chem. Phys.*, *4*, 627–638.

Plane, J. M. C., R. M. Cox, J. Qian, W. M. Pfenninger, G. C. Papen, C. S. Gardner, and P. J. Espy (1998), Mesospheric Na layers at extreme high latitudes in summer, *J. Geophys. Res.*, *103*, 6381–6389.

Plane, J. M. C., C. S. Gardner, J. Yu, C. Y. She, R. R. Garcia, and H. C. Pumphrey (1999a), Mesospheric Na layer at 40°N: Modeling and observations, *J. Geophys. Res.*, *104*, 3773–3788.

Plane, J. M. C., R. M. Cox, and R. J. Rollason (1999b), Metallic layers in the mesopause and low thermosphere region, *Adv. Space Res.*, *24*, 1559–1570.

Plane, J. M. C., D. E. Self, T. Vondrak, and K. R. I. Woodcock (2003), Laboratory studies and modeling of mesospheric iron chemistry, *Adv. Space Res.*, *32*, 699–708.

Plane, J. M. C., B. J. Murray, X. Z. Chu, and C. S. Gardner (2004), Removal of meteoric iron on polar mesospheric clouds, *Science*, *304*, 426–428.

Raizada, S., and C. A. Tepley (2003), Seasonal variation of mesospheric iron layers at Arecibo: First results from low-latitudes, *Geophys. Res. Lett.*, *30*(2), 1082, doi:10.1029/2002GL016537.

Shimazaki, T. (1985), *Minor Constituents in the Middle Atmosphere*, Springer, New York.

Simonich, D. M., B. R. Clemesha, and V. W. H. Kirchhoff (1979), The mesospheric sodium layer at 23°S: Nocturnal and seasonal variations, *J. Geophys. Res.*, *84*, 1543–1550.

States, R. J., and C. S. Gardner (1999), Structure of the mesospheric Na layer at 40°N latitude: Seasonal and diurnal variations, *J. Geophys. Res.*, *104*, 11,783–11,798.

Thomas, G. E. (1991), Mesospheric clouds and the physics of the mesopause region, *Rev. Geophys.*, *29*, 553–575.

von Zahn, U., and U. Berger (2003), Persistent ice cloud in the midsummer upper mesosphere at high latitudes: Three-dimensional modeling and cloud interactions with ambient water vapor, *J. Geophys. Res.*, *108*(D7), 8451, doi:10.1029/2002JD002409.

von Zahn, U., G. Hansen, and H. Kurzawa (1988), Observations of the sodium layer at high latitudes in summer, *Nature*, *331*, 594–596.

Yrjola, I., and P. Jenniskens (1998), Meteor stream activity–VI. A survey of annual meteor activity by means of forward meteor scattering, *Astron. Astrophys.*, *330*(2), 739–752.

———————————

X. Chu and C. S. Gardner, Department of Electrical and Computer Engineering, University of Illinois at Urbana-Champaign, Urbana, IL 61801, USA. (cgardner@uiuc.edu)

B. J. Murray, Department of Chemistry, University of British Columbia, 2036 Main Mall, Vancouver, British Columbia V6T 1Z1, Canada.

W. Pan, Center for Geospace Studies, SRI International, 333 Ravenswood Avenue, Menlo Park, CA 94025-3493, USA.

J. M. C. Plane and T. Vondrak, School of Environmental Sciences, University of East Anglia, Norwich NR4 7TJ, UK.